University of Reading

Nonlinear rheology and dynamics of supramolecular polymer networks formed by associative telechelic chains under shear and extensional flows

Article

Supplemental Material

It is advisable to refer to the publisher's version if you intend to cite from the work. See Guidance on citing.

www.reading.ac.uk/centaur

CentAUR

Central Archive at the University of Reading

Reading's research outputs online

Supplementary Material

Nonlinear Rheology and Dynamics of Supramolecular Polymer Networks Formed by Associative Telechelic Chains Under Shear and Extensional Flows

Dipesh Amin and Zuowei Wang*

School of Mathematical, Physical and Computational Sciences, University of Reading, Whiteknights, PO Box 220, Reading RG6 6AX, UK

S1 Transient shear and extensional viscosities of weakly entangled polymer systems

Figures S1 and S2 present our simulation results on the transient viscosities of the weakly entangled melt and SPN systems with chain length $N = 128$ obtained in stratup shear and extensional flows, respectively. These results are discussed in the main text together with the simulation data obtained from the unentangled systems with $N = 45$ (Figures 2 and 5 therein).

S2 Stress-strain curves obtained in startup flows

Figures S3 and S4 present our simulation results on the transient shear stresses, σ_{xy}, and extensional tensile stresses, $\sigma_{xx} - \sigma_{yy}$, of the melt and SPN systems with two different chain lengths as functions of strain $\gamma = \dot{\gamma}t$ and $\epsilon = \dot{\epsilon}t$, respectively. The stress data for the systems with $N = 45$ are the same as those presented in Figures 2 and 5 of the
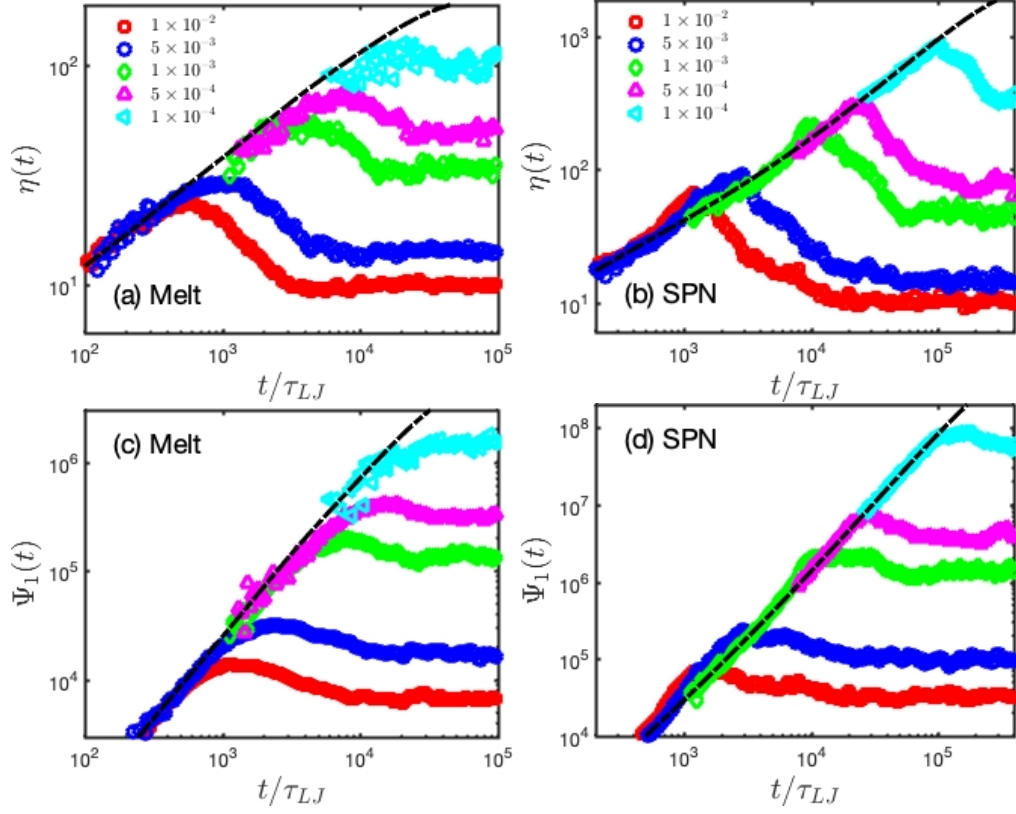
Figure S1: Transient shear viscosities, $\eta(t)$, and first normal stress coefficients, $\Psi_1(t)$, obtained from shear simulations of the melts (a,c) and supramolecular polymer networks (b,d) with chain length $N = 128$ at different dimensionless shear rates $\dot{\gamma}\tau_{LJ}$. The black dot-dashed lines are the linear viscosities, $\eta^+(t)$, and linear first normal stress coefficients, $\Psi_1^+(t)$, calculated in equilibrium simulations of the corresponding systems. The studied dimensionless shear rates $\dot{\gamma}\tau_{LJ}$ are given in the legends.
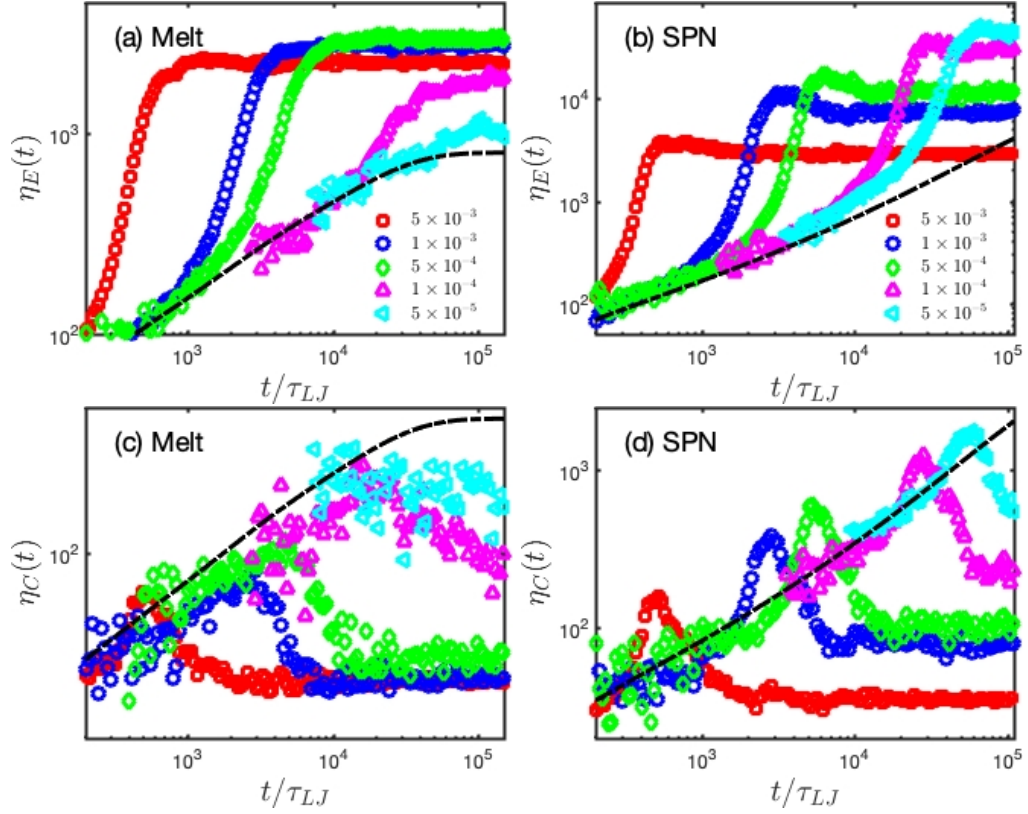
Figure S2: Transient planar extensional viscosities, $\eta_E(t)$, and cross viscosities, $\eta_C(t)$, obtained from planar extension simulations of the melt (a,c) and SPN (b,d) systems with chain length $N = 128$ at different dimensionless extension rates $\dot{\epsilon}\tau_{LJ}$. The black dot-dashed lines represent the linear planar extensional and cross viscosities estimated as $Tr\eta^+(t)$ with the Trouton ratios $Tr = 4$ for $\eta_E(t)$ and 2 for $\eta_C(t)$. The studied dimensionless extension rates $\dot{\epsilon}\tau_{LJ}$ are given in the legends.
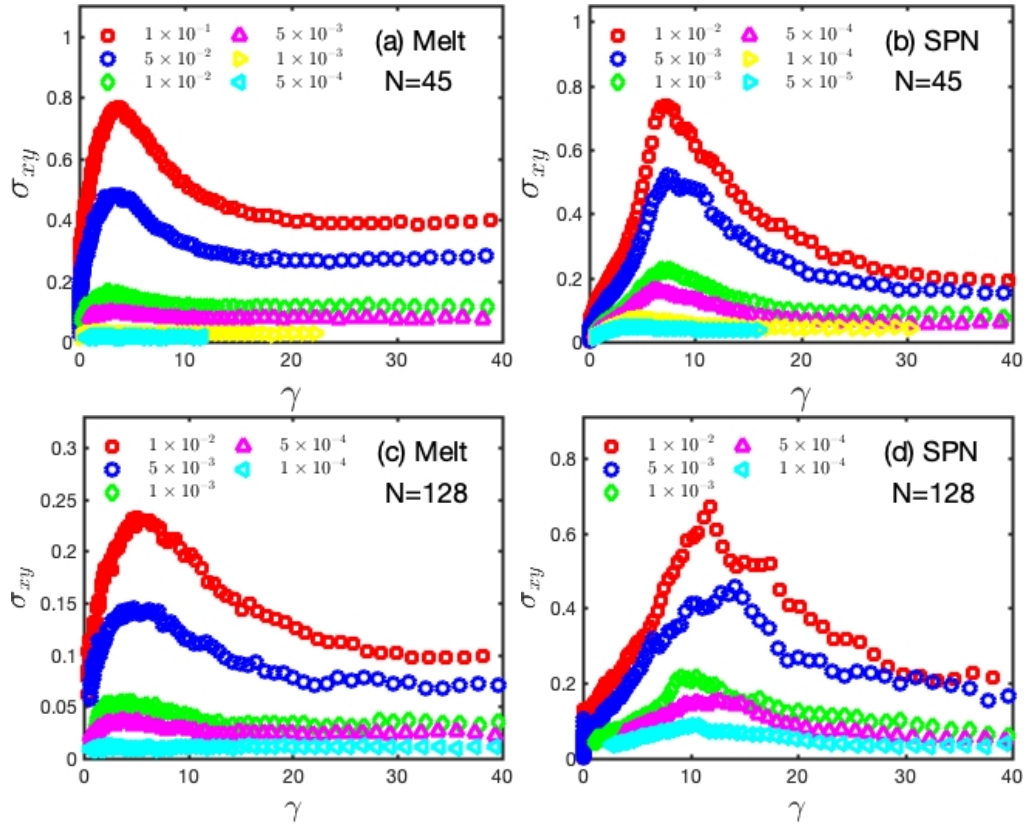
Figure S3: Transient shear stresses, $\sigma(\gamma)$, obtained from startup shear simulations of the melt (a,c) and SPN (b,d) systems with chain lengths $N = 45$ and 128 as functions of the shear strain $\gamma = \dot{\gamma}t$, respectively. The studied dimensionless shear rates $\dot{\gamma}\tau_{LJ}$ are given in the legends.
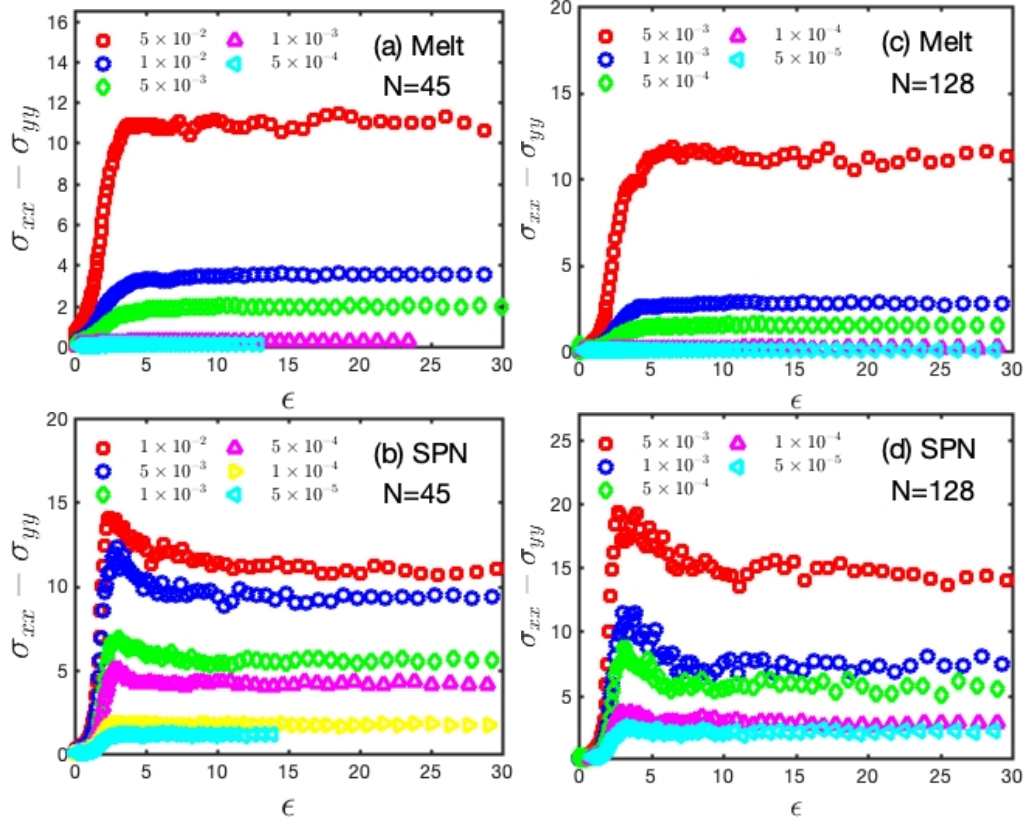
Figure S4: Transient tensile stresses, $\sigma_{xx}(\epsilon) - \sigma_{yy}(\epsilon)$, obtained from startup extensional simulations of the melt (a,b) and SPN (c,d) systems with chain lengths $N = 45$ and 128 as functions of the extension strain $\epsilon = \dot{\epsilon}t$, respectively. The studied dimensionless extension rates $\dot{\epsilon}\tau_{LJ}$ are given in the legends.
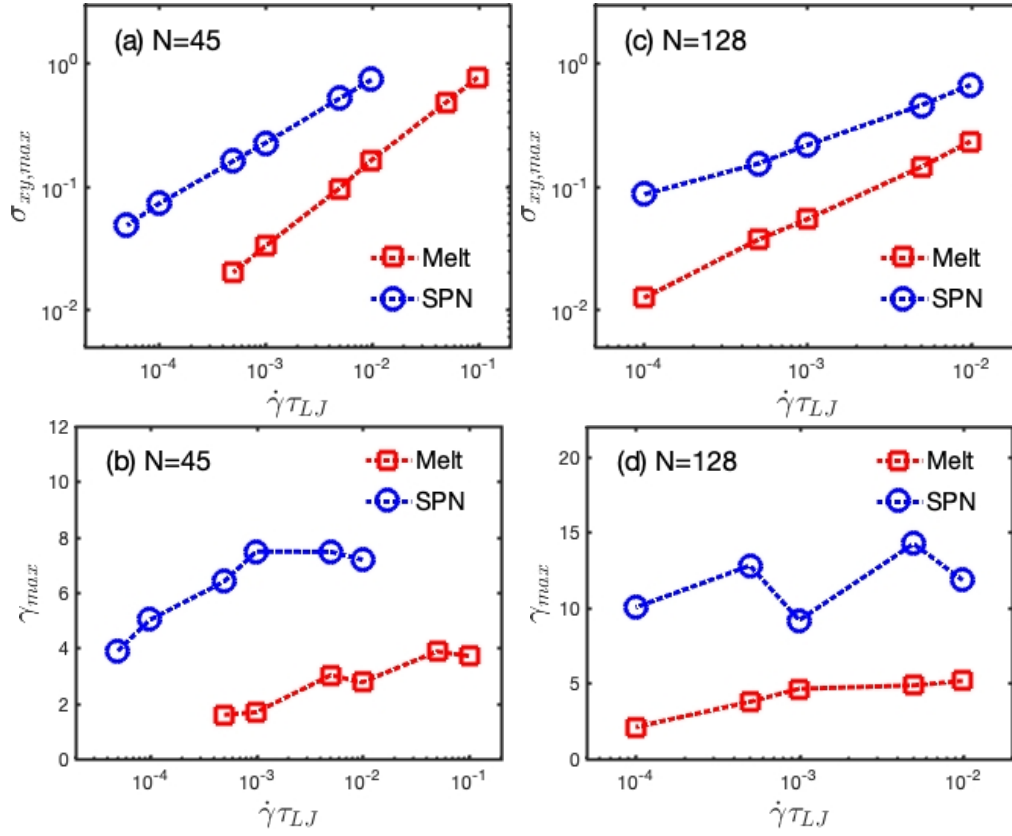
Figure S5: Stress maxima, $\sigma_{xy,max}$, and the corresponding strain locations, γ_{max}, in the shear stress-strain curves presented in Figure S3 shown as functions of the dimensionless shear rate.

main text, but replotted as functions of strain instead of time. The $\sigma_{xy}(\gamma)$ results for the unentangled SPN systems in Fig. S3(b) are qualitatively similar to the experimental data obtained from supramolecular networks formed by unentangled PIB-BA2 polymers.[1] Quantitative comparison between the simulation and experimental results is somewhat difficult due to different sticker association mechanisms and sticky bond lifetimes involved in the studied systems.

The stress maxima, $\sigma_{xy,max}$, and the corresponding strain locations, γ_{max}, in the shear stress-strain curves presented in Fig. S3 are shown in Figure S5 as functions of the dimensionless shear rate. It can be seen that for all polymer systems we simulated $\sigma_{xy,max}$ increases monotonically with the increase of the shear rate. The location γ_{max} of the stress maximum also shows a general trend to shift to higher values with increasing $\dot{\gamma}$, apart from the weakly entangled SPNs with $N = 128$ where the data are too noisy to draw a solid conclusion. For unentangled SPNs, this trend is consistent with the experimental observation of Yan *et al.*[1]

S3   Chain tumbling under shear

We have calculated the autocorrelation functions of the unit end-to-end vectors $\hat{\mathbf{R}}_{ee}$ of the polymer chains in the steady state of the shear flows[2,3]

$$\Phi(t) = < \hat{\mathbf{R}}_{ee}(t) \cdot \hat{\mathbf{R}}_{ee}(0) > \tag{S1}$$

for characterizing the possible chain tumbling behavior. Fig. S6 presents the simulation results on $\Phi(t)$ of the unentangled melt and SPN systems with chain length $N = 45$ at two different shear rates. $\Phi(t)$ of the melt system obtained at $\dot{\gamma}\tau_{LJ} = 10^{-2}$ shows the damped oscillatory behavior, indicating the existence of chain tumbling behavior. But there are no enough oscillation periods to provide a good fit to the damped periodic oscillation function[2,3]

$$\Phi(t) = A \exp(-t/\tau_{long}) \cos(2\pi t/\tau_{rot}) \tag{S2}$$

7

where τ_{long} and τ_{rot} are the longest relaxation time and the tumbling period of the chain, respectively. Apparently much higher shear rates are needed for the chains to undergo periodic tumbling even in the melt systems. On the other hand, oscillation in $\Phi(t)$ of the SPN systems is much weaker and hard to be characterized, which implies the suppression of tumbling behavior due to the transient network formation. The $\Phi(t)$ results of the melt and SPN systems with $N = 128$ show qualitatively very similar behavior.
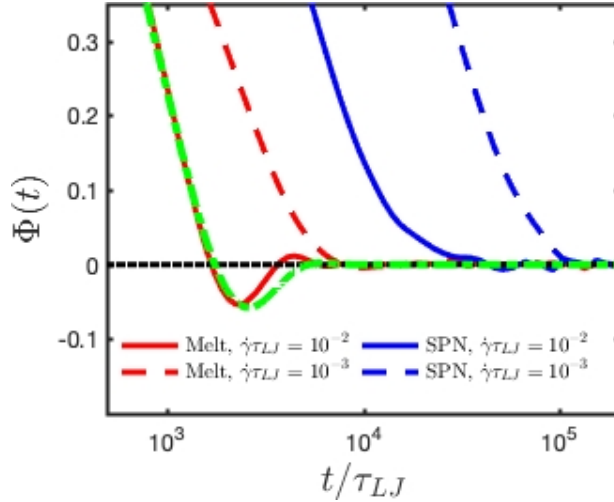

Figure S6: Autocorrelation functions $\Phi(t)$ of the unit end-to-end vectors of polymer chains in the melt and SPN systems with chain length $N = 45$ under shear with different shear rates $\dot{\gamma}$. The calculations were performed after the systems have entered the steady state. The green dotted-dashed line is the fitting of the $\Phi(t)$ data of the melt system to Eq. (S2).

S4   Fractions of associated chains in SPNs in steady state of shear flows

Figure S7 presents the simulation results on the average fractions of polymer chains which are in different association states, including free (none of the two end stickers associated), dangling (one end sticker associated and the other free), bridging (both

ends associated) and looping (two ends associated into the same sticker cluster) chains, in the unentangled SPNs with $N = 45$ under steady shear. Owing to the shear-induced reduction of the number of fully associated stickers (see Figure 8(a) in the main text), the fraction of bridging chains, which are elastically active, decreases from 97.3% at $\dot{\gamma}\tau_{LJ} = 10^{-4}$ to 90.3% at $\dot{\gamma}\tau_{LJ} = 10^{-2}$. Correspondingly, the fraction of dangling chains increases from about 1% to 7.2% over the same range of shear rates. The number of free chains remains to be extremely low (e.g., around 0.25% at $\dot{\gamma}\tau_{LJ} = 10^{-2}$) due to the relatively high sticker concentration in the studied SPN systems. It is noticed that the average fraction of looping chains fluctuates about $2.0 \pm 0.4\%$ in the $\dot{\gamma}$ range we studied, implying that there is no evident shear-induced conversion of looping chains to bridging (elastically active) chains. This can explain the absence of steady-state shear thickening in the SPN systems studied in the current work.
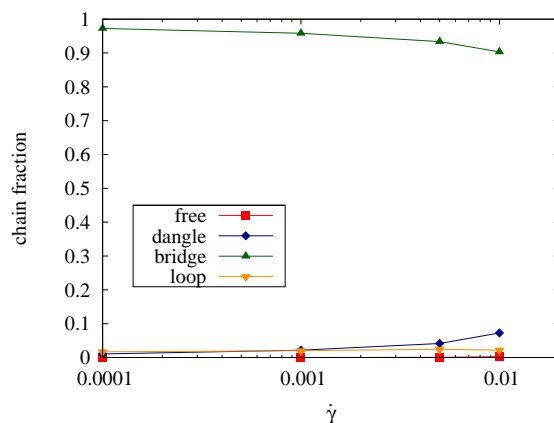

Figure S7: Average fractions of polymer chains in different association states in the SPNs with $N = 45$ in the steady state of shear flows. The shear rates have the unit of τ_{LJ}^{-1}.

S5   Chain stretching under steady extensional flow

To understand the simulation results on the steady-state chain stretching ratio λ presented in Figure 9(c) of the main text, we have calculated the probability distributions

of the chain end-to-end distances, $P(R_{ee})$ where $R_{ee} = <\boldsymbol{R}_{ee}^2>^{1/2}$, in both the melt and SPN systems with $N = 128$ under extensional flows. The analysis results are presented in Figure S8. It can be seen that at each given extensional rate $P(R_{ee})$ of the SPN has a much broader distribution with the maximum located at a higher R_{ee} value than that of the non-associative melt. This can be understood from the three-dimensional (3D) transient network formation in which the sticker clusters cross-link the telechelic chains into many different configurations, including bridging, dangling, looping and free ones. As a result, the end-to-end distances of the polymer chains can vary from $R_{ee} \sim \sigma_{LJ}$ for a looping chain to $R_{ee} \sim N\sigma_{LJ}$ for a fully stretched bridging chain. The bridging chains can sustain high stretching forces, leading to the extension of $P(R_{ee})$ to high R_{ee} side. At low and intermediate extensional rates ($\dot{\epsilon}\tau_{LJ} \leq 10^{-3}$), both the average R_{ee} value and the extensional viscosity of a SPN system are higher than those of its melt counterpart as expected.
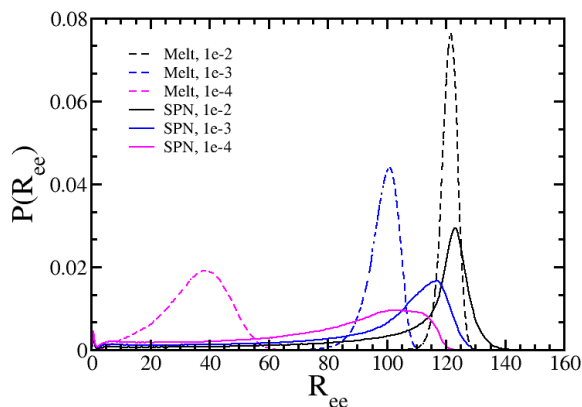

Figure S8: Probability distributions of the chain end-to-end distances, $P(R_{ee})$, in the melt and SPN systems with $N = 128$ at different dimensionless extensional rates $\dot{\epsilon}\tau_{LJ}$. The results were obtained after the systems have entered the steady state.

At high extensional rates (e.g., $\dot{\epsilon}\tau_{LJ} = 10^{-2}$ in Fig. S8) $P(R_{ee})$ of the melt with $N = 128$ shows a narrow distribution around the peak at $R_{ee} \approx 121\sigma_{LJ}$, indicating that nearly all of the non-associative polymer chains are fully stretched and aligned along
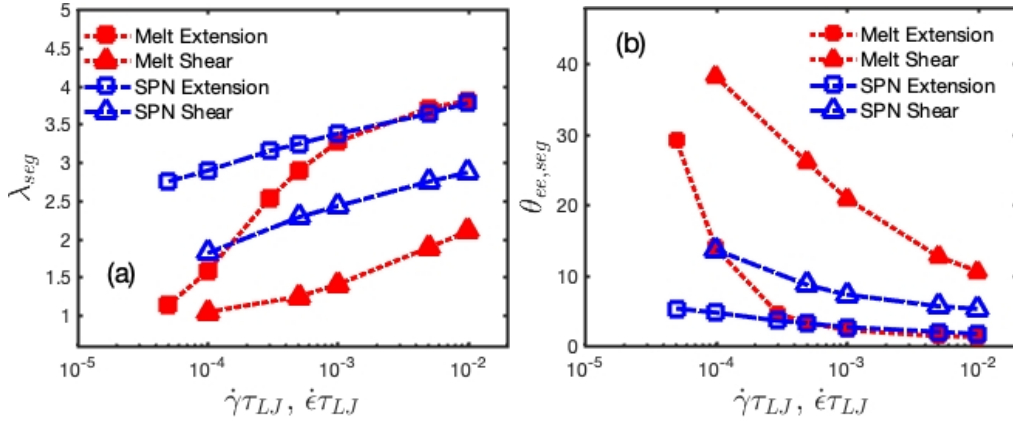
Figure S9: (a) Average stretching ratio, λ_{seg}, and (b) average end-to-end vector orientation angle with respect to the shear or elongation directions, $\Theta_{ee,seg}$, of chain segments with length $N_{seg} = 25$ in the melt and SPN systems with $N = 128$. The results were calculated in the steady state of the shear and extensional flows by averaging over the middle 50 monomers of each polymer chain.

the elongation direction. On the other hand, $P(R_{ee})$ of the SPN system still demonstrates a broad distribution with the peak located at $R_{ee} \approx 123\sigma$ and its tail extending to higher R_{ee} beyond that of the melt. There are thus a number of highly stretched associative chains in the SPN which carry higher stretching forces than those in the melt. Moreover, the associative chains with small end-to-end distances are typically not of the compact coil-like conformations. Instead they take piecewise-stretched bending or folding configurations which are tightly hooked with other chains at the bending or hairpin points. This can be seen in Fig. S9 from the simulation results on the stretching ratio, $\lambda_{seg} = R_{ee,seg}(t)/R^0_{ee,seg}$, and end-to-end vector orientation angle, $\Theta_{ee,seg}$ of chain segments with length $N_{seg} = 25$. These results were obtained by averaging over the middle 50 monomers of each chain. The equilibrium end-to-end distance of the segments is estimated as $R^0_{ee,seg} = (N_{seg} - 1)^{1/2}b$ where b is the statistical bond length. The agreement between the λ_{seg} and $\Theta_{ee,seg}$ data of the SPN and melt systems at high extension rates indicates that the chain segments in both systems are highly stretched and oriented to very similar magnitudes. The contribution of the local chain segment

11

stretching to the tensile stress is not sufficiently reflected in the average chain stretching ratio λ presented in Figure 8(c) of the main text. Therefore the extensional viscosities of the SPNs at high extension rates can still be larger than those of their melt counterparts, even though their average chain stretching ratios might be somewhat smaller than the latter.

As an additional remark, the simulation results obtained from the polymer systems with relatively long chains at high extensional rates may also be affected by the usage of the FENE chain model and the SLLOD method, which are subject to further studies.
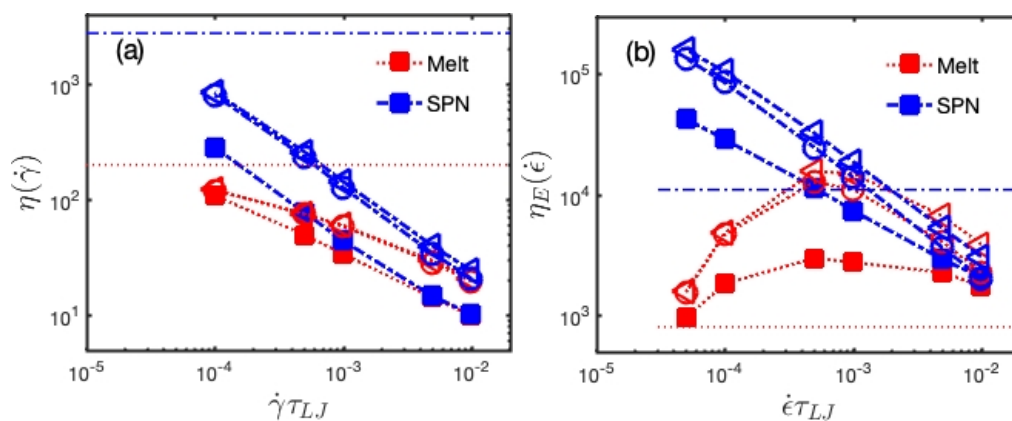

Figure S10: Comparison of the predictions of the decoupling approximation on the steady-state shear (a) and extensional (b) viscosities with the results directly obtained from the simulations for the melt and SPN systems with chain length $N = 128$. In (a) the circle and triangle symbols represent the approximations obtained using Eq. 18 and Eq. 19 in the main text, respectively. The results in (b) are obtained by replacing σ_{xy} and S_{xy} in Eqs 18 and 19 with $\sigma_{xx} - \sigma_{yy}$ and $S_{xx} - S_{yy}$.

S6   Steady-state shear and extensional viscosities: Test of decoupling assumption

In Figure S10(a), we compare the predictions made by using Eqs. 18 and 19 in the main text on the steady-state shear viscosities $\eta(\dot{\gamma})$ of the melt and SPN systems with chain

12

length $N = 128$ with those directly calculated in the simulations. The simulation data on the chain stretching ratio $\lambda(t)$ and the segment orientation tensor element $S_{xy}(t)$ obtained in the steady-state shear flows have been used as inputs for Eqs. 18 and 19. Fig. S10(b) presents similar comparison for the steady-state extensional viscosities $\eta_E(\dot{\epsilon})$ of these polymer systems, where the predictions were made by replacing σ_{xy} and S_{xy} in Eqs. 18 and 19 with $\sigma_{xx} - \sigma_{yy}$ and $S_{xx} - S_{yy}$, respectively. Again simulation results on $\lambda(t)$ and $S_{xx}(t) - S_{yy}(t)$ obtained in the steady-state planar extensional flows were used as inputs for making the predictions.
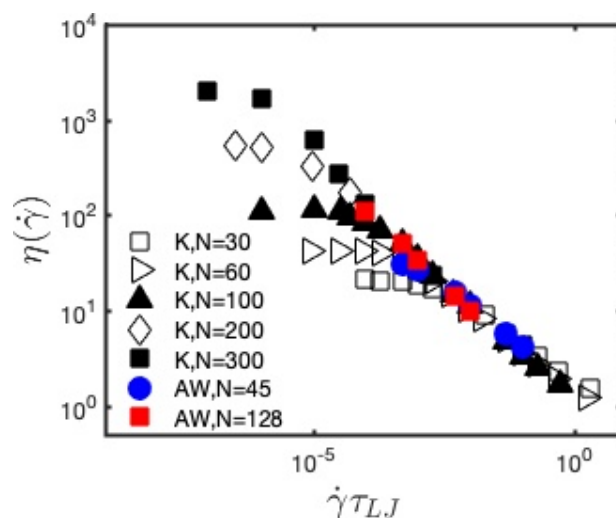

Figure S11: Comparison of steady-state shear viscosities of melt systems obtained in the current work (marked as AW) with those extracted from Figure 1(a) of Ref.[4] by Kröger *et al.* (marked as K).

S7   Steady-state shear viscosities of melts: A comparison with other simulation data

Figure S11 compares our simulation results on the steady-state shear viscosities, $\eta(\dot{\gamma})$, of the non-associative melt systems with those reported by Kröger *et al.* in Figure 1(a) of their 2006 PRL paper.[4] A good agreement has been reached between the simulation

data obtained in the two different groups.

References

[1] Yan, T.; Schröer, K.; Herbst, F.; Binder, W. H.; Thurn-Albrecht, T. *Macromolecules* **2017**, *50*, 2973–2985.

[2] Kim, J.; Edwards, B.; Keffer, D.; Khomami, B. *Physics Letters A* **2009**, *373*, 769 – 772.

[3] Sefiddashti, M. H. N.; Edwards, B. J.; Khomami, B. *J. Rheol.* **2015**, *59*.

[4] Kröger, M.; Hess, S. *Phys. Rev. Lett.* **2000**, *85*, 1128–1131.